Journal of Materials Chemistry C

PAPER

View Article Online
View Journal

Cite this: DOI: 10.1039/c5tc02472b

Pyrimido[4,5-*g*]quinazoline-4,9-dione as a new building block for constructing polymer semiconductors with high sensitivity to acids and hole transport performance in organic thin film transistors†

Jesse Quinn, Chang Guo, Bin Sun, Adrian Chan, Yinghui He, Edward Jin and Yuning Li*

Received 8th August 2015,
Accepted 24th October 2015

DOI: 10.1039/c5tc02472b

www.rsc.org/MaterialsC

Pyrimido[4,5-*g*]quinazoline-4,9-dione (PQ) was used for the first time as a building block for π-conjugated polymer semiconductors. Copolymers of PQ and bithiophene showed dramatic bathochromic shifts in their absorption spectra in the presence of protonic (acetic acid and trifluoroacetic acid) and Lewis (BBr_3) acids, resulting from the strong interaction of the basic 1,6-nitrogen atoms in the PQ unit with the acid. These polymers exhibited characteristic p-type semiconductor performance with hole mobilities of up to 6.4×10^{-3} cm^2 V^{-1} s^{-1} in organic thin-film transistors (OTFTs). The potential bioactivity, high sensitivity to acids, and good field effect transistor performance of these PQ-based polymers will enable their application for bio- and chemo-sensors.

Introduction

π-Conjugated polymers have been extensively studied in the past two decades as channel semiconductors for printed organic thin film transistors (OTFTs), which are potentially active elements for many electronics such as radio-frequency identification (RFID) tags, flexible displays, memory devices, biological and chemical sensors, *etc.*[1–7] Charge carrier mobility of polymer semiconductors has greatly improved in the past few years largely due to the development of new building blocks.[8–11] Amide/imide-containing building blocks such as naphthalene-bisdicarboximide (NDI),[12] 1,4-diketopyrrolo[3,4-*c*]pyrrole (DPP),[13] (*E*)-[3,3′-biindolinylidene]-2,2′-dione or isoindigo (IID),[14] and (3*E*,7*E*)-3,7-bis(2-oxoindolin-3-ylidene)benzo[1,2-*b*:4,5-*b*′]difuran-2,6(3*H*,7*H*)-dione (IBDF)[15,16] have drawn tremendous attention since polymer semiconductors based on these building blocks have shown remarkable charge transport performance in OTFTs.

Here, we introduce a new amide-containing building block, pyrimido[4,5-*g*]quinazoline-4,9-dione (PQ), for polymer semiconductors. PQ is a large π-conjugated fused ring structure comprising of two pyrimidinones and a central benzo core. We were particularly interested in this building block because of the bioactivities of the quinazoline-4(3*H*)-one moiety. Quinazolin-4(3*H*)-one derivatives have gained considerable attention as potential therapeutic medicines for treatment of various diseases.[17–22] Furthermore, the 1,6-nitrogen atoms in PQ possess available electron lone pairs (basic) to interact with acids. Therefore, we expect that PQ-based polymers may exhibit activities towards biological substances and acids and can be used in OTFTs for chemo- and bio-sensing applications.[23–25]

Although PQ derivatives were reported as early as in the 1900s by Bogert *et al.*,[26,27] synthetic approaches to PQ compounds have not been well established yet.[28–31] We recently reported a facile method in synthesizing PQ-based compounds.[32] In this work, we used the bromo-functionalized compounds (**PQ2T-R-Br**) in Scheme 1 as monomers to successfully synthesize two PQ-based π-conjugated polymers. These polymers demonstrated promising p-type semiconductor performance in OTFTs and interesting responses in their UV absorption profiles to protonic and Lewis acids.

Results and discussion

Our study began with conducting theoretical calculations by density functional theory (DFT) through Gaussian 09 Revision D.01[33] using the functional B3LYP and the basis set 6-31G(d) under tight convergence to investigate the geometry, molecular energy levels, and electron distributions of a simple 2,7-dithienyl-substituted PQ molecule, **PQ2T-Me** (Fig. 1). The modelling results showed that the PQ unit is nearly coplanar with the pyrimidinone rings to be slightly raised off by 2–3° due to steric effects from the

Department of Chemical Engineering and Waterloo Institute for Nanotechnology (WIN), University of Waterloo, 200 University Ave West, ON, Waterloo, N2L 3G1, Canada. E-mail: yuning.li@uwaterloo.ca; Fax: +1-519-888-4347; Tel: +1-519-888-4567 ext. 31105

† Electronic supplementary information (ESI) available: Details of computer simulations, NMR, DSC, and additional OTFT data. See DOI: 10.1039/c5tc02472b

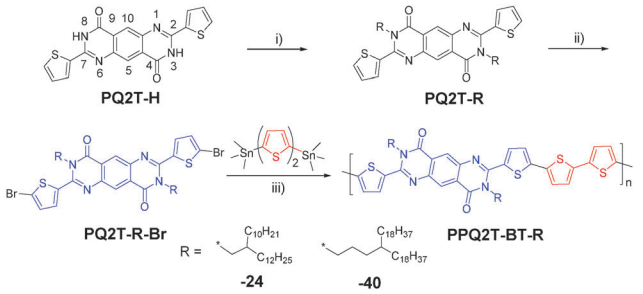

Scheme 1 The synthetic route to **PPQ2T-BT-R** polymers. *Reagents and conditions*: (i) K_2CO_3/DMF/130 °C; (ii) NBS/chloroform; (iii) $Pd_2(dba)_3$/P(*o*-tolyl)$_3$/chlorobenzene/130 °C.

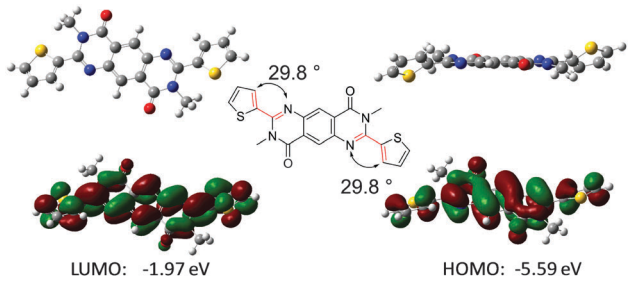

Fig. 1 Optimized geometry and HOMO and LUMO energy levels for **PQ2T-Me** obtained by DFT calculations with B3LYP/6-31G(d).

neighbouring thiophene rings. A large dihedral angle of ~30° between the PQ unit and thiophene was observed. The lowest unoccupied molecular orbital (LUMO) and highest occupied molecular orbital (HOMO) wavefunctions are evenly distributed throughout the molecule. The LUMO and HOMO energy levels of **PQ2T-Me** were calculated to be −1.97 and −5.59 eV, respectively. To gain further insight into the polymer properties, the dimer of **PQ2T-BT-Me** was simulated (ESI†). The LUMO and HOMO energy levels were calculated to be −2.57 and −5.17 eV, respectively. The HOMO wavefunction is evenly distributed across the dimer, while the LUMO wavefunction is localized to the thiophene units. The dihedral angles between the PQ unit and thiophene units were slightly lower (~27°) than that calculated for **PQ2T-Me**. The result suggests that the LUMO is mostly influenced by the thiophene units in the dimer.

2,7-Di(thiophen-2-yl)-3,8-dihydropyrimido[4,5-*g*]quinazoline-4,9-dione (**PQ2T-H**), which was prepared *via* our previously established synthetic route,[32] was substituted with 2-decyltetradecyl or 4-octadecyldocosanyl to obtain **PQ2T-24** (73% yield) or **PQ2T-40** (67% yield), respectively (Scheme 1). Subsequently, **PQ2T-24** and **PQ2T-40** were brominated with *N*-bromosuccinimide (NBS) to obtain **PQ2T-Br-24** (75% yield) and **PQ2T-Br-40** (80% yield), respectively. Polymers **PPQ2T-BT-24** and **PPQ2T-BT-40** were synthesized *via* Stille coupling polymerization of **PQ2T-Br-24** and **PQ2T-Br-40**, respectively, with 5,5′-bis-(trimethylstannyl)-2,2′-bithiophene and purified using Soxhlet extraction. **PPQ2T-BT-24** was insoluble in chloroform and required further treatment with a high boiling point solvent, 1,1,2,2-tetrachloroethane (TCE). On the other hand, **PPQ2T-BT-40** was quite soluble in chloroform, which was due to its much larger side chains. The number average molecular weight (M_n) and polydispersity index (PDI) were measured to be 38.9 kg mol^{-1} and 3.68 for **PPQ2T-BT-24** and 43.5 kg mol^{-1} and 2.95 for **PPQ2T-BT-40**, respectively. Data were obtained using high-temperature gel-permeation chromatography (HT-GPC) at 140 °C with 1,2,4-trichlorobenzene as an eluent and polystyrene as standards. The thermal stability of these polymers was characterized using thermogravimetric analysis (TGA) (ESI†). **PPQ2T-BT-24** showed good thermal stability with a 5% weight loss temperature ($T_{-5\%}$) at 340 °C, while **PPQ2T-BT-40** showed slightly lower thermal stability with a $T_{-5\%}$ at 317 °C. No visible endothermic/exothermic transitions were observed on their differential scanning calorimetry (DSC) diagrams (ESI†).

PPQ2T-BT-24 in TCE showed a poorly resolved vibronic splitting absorption profile with the wavelength of maximum absorbance (λ_{max}) at 526 nm and a weak absorption shoulder at ~550 nm. The thin film exhibited a slight hypsochromic shift (λ_{max} = 522 nm) relative to that of solution (Fig. 2). **PPQ2T-BT-40** in chloroform showed a slightly better resolved vibronic splitting absorption pattern with λ_{max} at 562 nm accompanied by the appearance of an absorption shoulder at 531 nm. The thin film exhibited the same λ_{max} at 562 nm with a more resolved absorption shoulder at 524 nm. The larger λ_{max} observed for **PPQ2T-BT-40** both in solution and film compared to **PPQ2T-BT-24** is considered due to the farther distance of the bifurcation point of C40 side chain in the former, which allows for achieving higher coplanarity of the polymer backbone.[34] The hypsochromic shift from solution to film observed for **PPQ2T-BT-24** can be attributed to the H-aggregation over the J-aggregation as a result of the delicate competition between interchain coupling and intrachain coupling.[35,36] The optical band gap of **PPQ2T-BT-24** and **PPQ2T-BT-40** calculated from the onset absorption wavelengths of their thin films is ~2.03 eV.

Conjugated polymers containing pyridine,[37] imidazole,[38] benzimidazole,[39–41] quinoxaline,[41] phenanthroline,[37] benzothiadiazole,[42] and pyridalthiadiazole[42] have been reported to strongly interact with acids due to the available lone pairs on the nitrogen atoms in these moieties. Similarly, the in-plane electron lone pairs

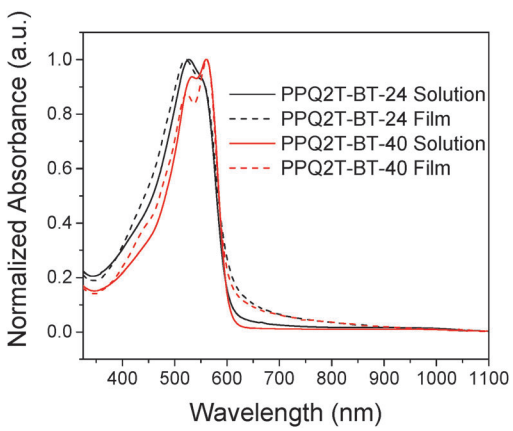

Fig. 2 UV-Vis-NIR absorption spectra of **PPQ2T-BT-24** and **PPQ2T-BT-40** in TCE and chloroform, respectively, and as thin-films on glass substrates.

of the nitrogen atoms at the 1 and 6 positions in the PQ moiety are not involved in π-conjugation, which would act as basic sites to interact with acids. To investigate the acid effects on these PQ polymers, a strong organic acid, trifluoroacetic acid (TFA: pK_a = −0.25)[43] and a weak organic acid, acetic acid (AcOH: pK_a = 4.8)[43] were chosen, because they are readily soluble in the organic solvent used (chlorobenzene) and their concentration can be easily controlled. As shown in Fig. 3A, at a TFA concentration as low as 10 μM, a level similar to that of the PQ units in **PPQ2T-BT-24** ($\sim 1 \times 10^{-5}$ M), a long wavelength shoulder at ~650 nm appeared. As the TFA concentration further increases, the λ_{max} bathochromically shifts. At a TFA concentration of 10 mM, no further spectral change occurs and a largest λ_{max} of 673 nm is reached, which corresponds to a bathochromic shift of 145 nm from that of the solution without acid. For the much weaker acid, AcOH, a very high concentration of 2 M was needed to make a noticeable spectral change (Fig. 3B). The largest λ_{max} of 634 nm, or a bathochromic shift of 106 nm from the solution without acid, was observed at an AcOH concentration of 5 M. Further increasing the AcOH concentration resulted in precipitation of the polymer since AcOH is a non-solvent for **PPQ2T-BT-24**. The smaller achievable bathochromic shift observed in AcOH than in TFA is most likely due to the lower H^+ concentration in the former, being unable to fully protonate the 1,6-nitrogen atoms in the polymer. To demonstrate binding of Lewis acids to the 1,6-nitrogen atoms, a strong Lewis acid, boron tribromide (BBr_3), was used (Fig. 3C). At a very low BBr_3 concentration of 1 μM, a shoulder appeared at ~650 nm in the UV-Vis-NIR spectrum of **PPQ2T-BT-24**, similar to the solution

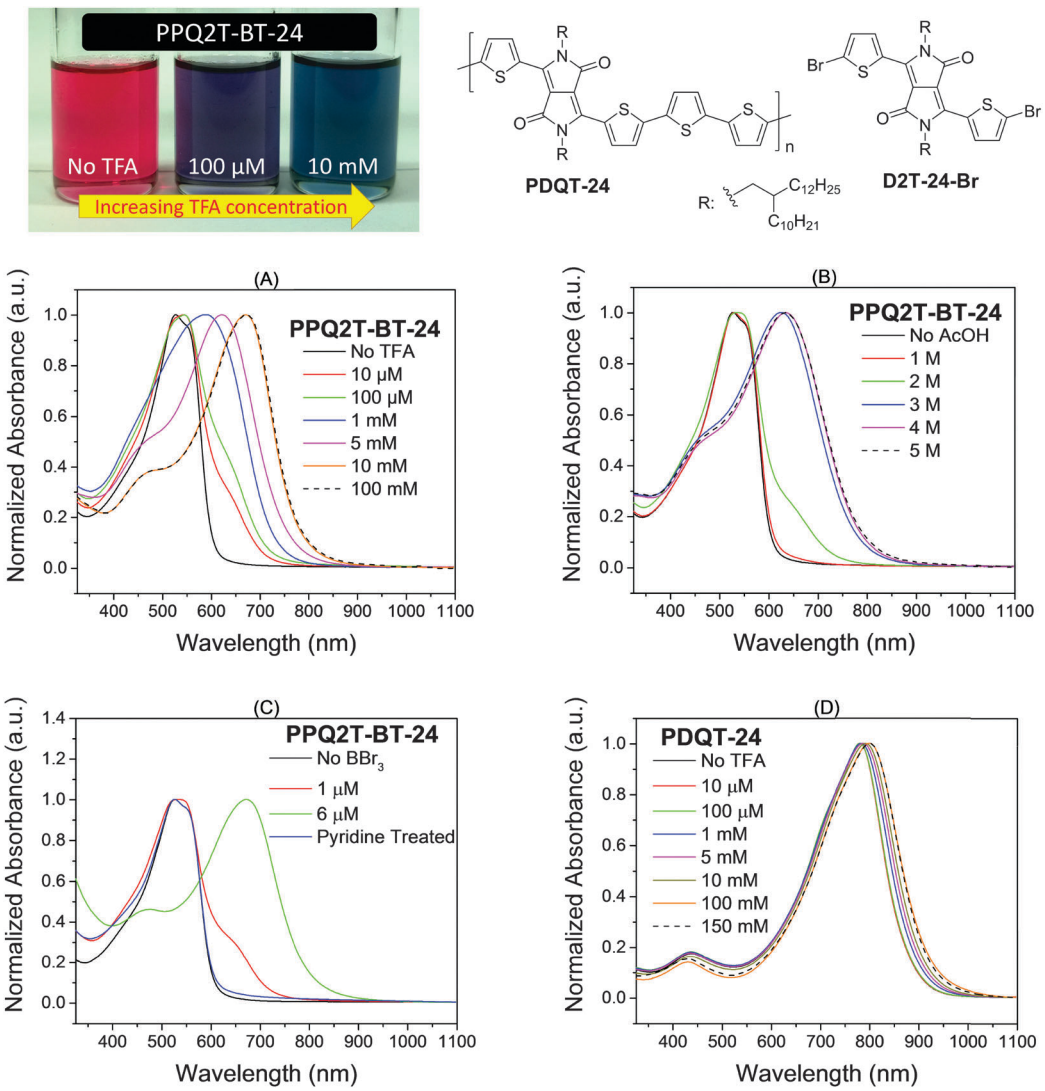

Fig. 3 Top left: Colour change of **PPQ2T-BT-24** solutions with increasing concentration of trifluoroacetic acid (TFA) from 0 M (left), to 10^{-4} M (middle) and 10^{-2} M (right) with a molar concentration of the polymer repeat unit at $\sim 1 \times 10^{-5}$ M. Top right: Structure of diketopyrrolopyrrole (DPP)-quaterthiophene copolymer with 2-decyltetradecyl side chain (**PDQT-24**) and its monomer (**D2T-24-Br**).[34] (A–C) show the UV-Vis-NIR absorption spectra of **PPQ2T-BT-24** in chlorobenzene with various concentrations of TFA, AcOH, and BBr_3, respectively, (D) shows the UV-Vis-NIR absorption spectra of **PDQT-24** in chlorobenzene with various concentrations of TFA. The measurements were conducted under nitrogen with a molar concentration of the polymer repeat unit at $\sim 1 \times 10^{-5}$ M.

containing TFA, but the latter required a much higher acid (TFA) concentration of ~10 μM, which is due to the stronger acidity of BBr_3. At a BBr_3 concentration of 6 μM the absorption spectrum bathochromically shifted with a λ_{max} of 673 nm, which appears to be identical to that of the longest λ_{max} obtained in the TFA solution at ~10 mM. Greater concentrations of BBr_3 lead to precipitation of the polymer–BBr_3 complexes. It should be noted that the spectral changes are reversible; the original spectra of the pristine polymers could be recovered by adding a base such as pyridine (Fig. 3C) to neutralize the acid in the polymer solution. Similar responses to TFA, AcOH, and BBr_3 were observed for **PPQ2T-BT-40** (ESI†) although the largest λ_{max} obtained in TFA, AcOH, and BBr_3 are at longer wavelengths of 659 nm, 686 nm, and 707 nm, respectively, which result from the more coplanar backbone of **PPQ2T-BT-40** as discussed above.

Two other nitrogen atoms at the 3,8-position in PQ, which reside in the amide moieties, are not expected to strongly interact with acids because typical amides are very weak bases with their conjugate acids having a pK_a value of ~1.[44] To demonstrate that the basic 1,6-nitrogen atoms are mainly responsible to the marked bathochromic shifts in the presence of acids, a diketopyrrolopyrrole (DPP)-quaterthiophene copolymer with the same 2-decyltetradecyl side chain (**PDQT-24**, Fig. 3),[34] was tested at various concentrations of TFA for comparison (Fig. 3D). **PDQT-24** contains amide nitrogen atoms in the DPP unit, which are similar to the 3,8-nitrogen atoms in the PQ unit. As expected, only a subtle bathochromic shift of ~3 nm was observed in 1 mM TFA solution and the maximum bathochromic shift of ~20 nm was achieved at a TFA concentration of 150 mM, which is 15 times larger than that required for **PPQ2T-BT-24** (~10 mM TFA). To further corroborate the interaction of 1,6-nitrogen atoms in PQ with acids, a similar UV-Vis-NIR study was performed on the monomers **PQ2T-24-Br** and **D2T-24-Br** (the monomer for **PDQT-24** shown in Fig. 2) at various concentrations of TFA (Fig. 4). **PQ2T-24-Br** showed a small shoulder at ~460 nm at 1 mM of TFA and then a significant change at 5 mM. When the TFA concentration is ≥100 mM, the spectra remain unchanged, indicating that all 1,6-nitrogen atoms were protonated. The maximum bathochromic shift (determined from the first peaks from the right side) is ~39 nm. The changes in the shape and relative intensities of absorption peaks with increasing TFA concentration from 1 mM to 100 mM are considered due to the formation of varied amounts of mono- and di-protonated species. On the contrary, **D2T-24-Br** showed no changes in peak positions when the TFA concentration was increased up to as high as 2 M. Variations in the relative intensities of some peaks are observed, which might be due to the solvent effect of TFA on **D2T-24-Br** molecules, since the polarity of TFA is much higher than the bulk solvent chlorobenzene and TFA is a poor solvent for **D2T-24-Br**. These results support that the 1,6-nitrogen atoms in the PQ units of **PPQ2T-BT-24** and **PPQ2T-BT-24** predominantly contribute to the large bathochromic shifts in the presence of acids. It is also noticed that the monomeric compound **PQ2T-24-Br** requires a two order of magnitude higher concentration (~1 mM) to make a notable change in its absorption spectrum compared with its polymer **PPQ2T-BT-24**

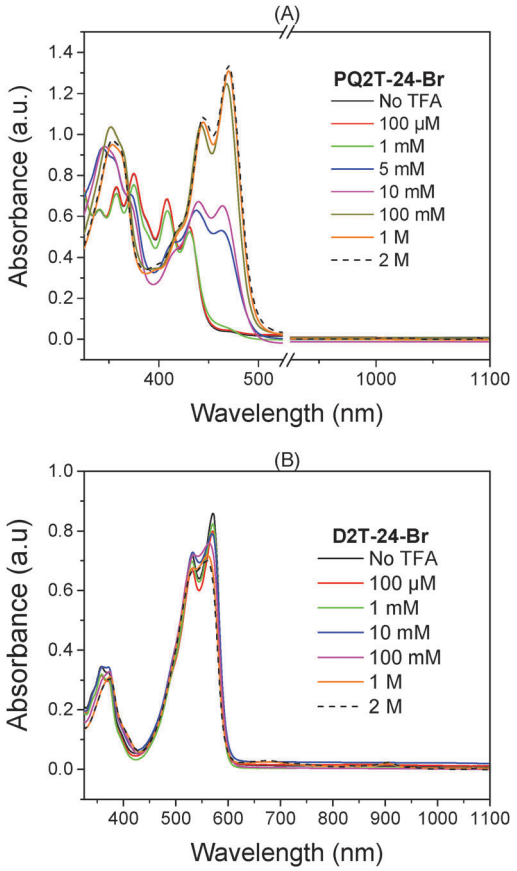

Fig. 4 The UV-Vis-NIR absorption spectra of (A) **PQ2T-24-Br** and (B) **D2T-24-Br** in chlorobenzene with various concentrations of TFA until little variation was observed. The measurements were conducted under nitrogen with a molar concentration of **PQ2T-24-Br** or **D2T-24-Br** at ~1×10^{-5} M.

(~10 μM), indicating that the polymer has greatly enhanced sensitivity towards an acid. It is assumed that protonation of one or a few PQ units would cause a notable change of the electronic state of the whole polymer main chain. This magnification effect might result from the extended delocalization of π-electrons along the polymer backbone as reported for other conjugated polymers that have been successfully used as highly sensitive chemosensors.[45]

Cyclic voltammetry (CV) measurements of polymer thin-films showed that **PPQ2T-BT-24** and **PPQ2T-BT-40** have HOMO levels of −5.30 eV and −5.29 eV, respectively, calculated from their oxidative onset potentials (ESI†). Neither of the two polymers showed reversible reductive processes. Hence, the LUMO energy levels were calculated from the HOMO energy levels obtained from the CV and the optical band gaps from the UV-Vis-NIR data to be equal to −3.27 eV for **PPQ2T-BT-24** and −3.26 eV for **PPQ2T-BT-40**.

To elucidate the molecular ordering of these polymers, reflection X-ray diffraction (XRD) measurements were performed with polymer thin films (~40 nm) spin coated on a SiO_2/Si wafer and annealed at 100, 150, and 200 °C. Both **PPQ2T-BT-24** and **PPQ2T-BT-40** only showed very low intensity diffraction peaks at

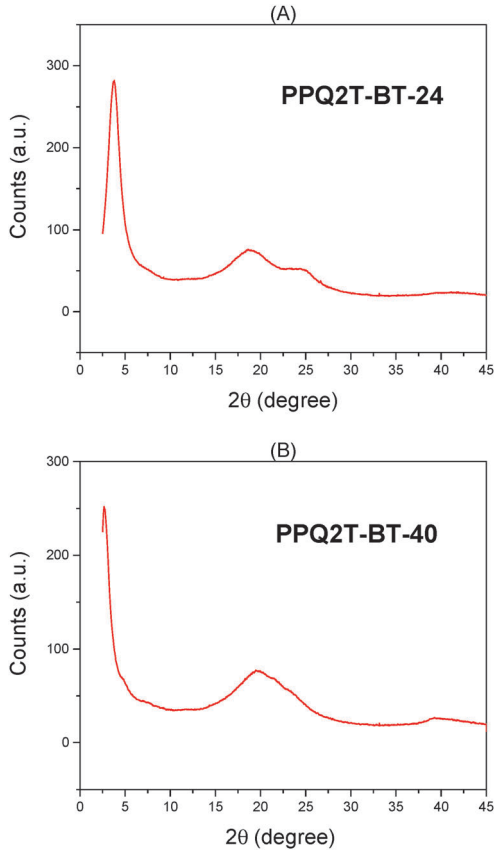

Fig. 5 The transmission XRD pattern (A) **PPQ2T-BT-24** and (B) **PPQ2T-BT-40** flakes stacked between two polyester film substrates with a Cu Kα (Rigaku) X-ray source (λ = 0.15406 nm).

low diffraction angles, indicating that the polymer thin films are rather disordered (ESI†). Transmission XRD measurements were also performed using thick polymer flakes (Fig. 5). **PPQ2T-BT-24** and **PPQ2T-BT-40** showed the primary (100) diffraction peaks at 2θ = 3.80° and 2.68°, which correspond to the inter-lamellar distances of 2.33 nm and 3.30 nm, respectively. The broad peak at 2θ = ~19–20° observed for **PPQ2T-BT-24** represents the van der Waals distance in the amorphous/disordered phase. The small hump centred at 2θ = 24.73° could be assigned to the (010) peak, originating from the co-facial π–π stacking distance of adjacent polymer backbones,[46] which was calculated to be 0.36 nm. However, **PPQ2T-BT-40** does not show a noticeable diffraction peak representing the π–π stacking distance due to the concurrent broad amorphous peak (2θ = ~19–20°) in the same region.

The film morphology of **PPQ2T-BT-24** and **PPQ2T-BT-40** thin-films spin-coated on dodecyltrichlorosilane modified SiO_2/Si wafer substrates was examined by atomic force microscopy (AFM). **PPQ2T-BT-24** thin films on DDTS-modified SiO_2/Si substrates showed poorly defined domains at all annealing temperatures tested, 100 °C, 150 °C, and 200 °C (ESI†). **PPQ2T-BT-40** films, especially for the 200 °C-annealed film, have more defined domains than the **PPQ2T-BT-24** films. The root mean square (RMS) roughness of the **PPQ2T-BT-40** films (~2 to 3 nm) is larger than that of the **PPQ2T-BT-24** films (<1 nm).

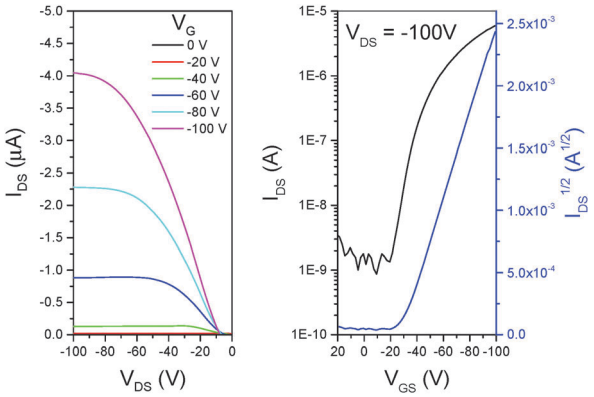

Fig. 6 Output (left) and transfer (right) curves of an OTFT device with a thin-film of **PPQ2T-BT-24** annealed at 250 °C. Device dimensions: channel length (L) = 30 μm; channel width (W) = 1000 μm.

The charge transport performance of **PPQ2T-BT-24** and **PPQ2T-BT-40** were evaluated in bottom-gate, bottom-contact OTFT devices using n++-doped conductive silicon wafer with a 300 nm-thick thermally grown SiO_2 dielectric layer as the substrate. Both polymers showed typical hole transport behaviour. Devices based on the 250 °C-annealed **PPQ2T-BT-24** films showed the best performance with the highest hole mobility of 6.4×10^{-3} cm^2 V^{-1} s^{-1} (Fig. 6) and an average value of 5.9×10^{-3} cm^2 V^{-1} s^{-1}. Devices based on **PPQ2T-BT-40** showed the best average mobility of 3.2×10^{-3} cm^2 V^{-1} s^{-1} with the highest value of 3.5×10^{-3} cm^2 V^{-1} s^{-1} for the films annealed at 300 °C (ESI†). The slightly higher hole mobility of **PPQ2T-BT-24** may be attributed to its slightly better film morphology. Our next step is to investigate the responses of the transistor characteristics (*e.g.*, I_{DS}, V_{th}, mobility, *etc.*) to the type and concentration of the acids exposed to and to explore the possibility of using the OTFTs based on these polymers for acid and bio sensors.

Experimental

Materials and instrumentation

All chemicals were purchased from commercial sources and used without further purification unless specified. 19-(3-Iodopropyl)-heptatriacontane,[47] 2,7-di(thiophen-2-yl)pyrimido[4,5-*g*]quinazoline-4,9(3*H*,8*H*)-dione[32] (**PQ2T-H**) and 2,7-bis(5-bromothiophen-2-yl)-3,8-bis(2-decyltetradecyl)-3,8-dihydropyrimido[4,5-*g*]quin-azoline-4,9-dione[32] (**PQ2T-Br-24**), and **PDQT-24** (M_n = 40.0 kg mol^{-1} and PDI = 3.22)[34] were synthesized according to the literature methods. GPC measurements were performed on a Malvern SEC system using 1,2,4-trichlorobenzene as eluent and polystyrene as standards at 140 °C. TGA measurements were carried out on a TA Instruments Q500 at a temperature ramping rate of 10 °C min^{-1} under nitrogen. DSC measurements were carried out on a TA Instruments Q2000 at a temperature ramping rate of 20 °C min^{-1} under nitrogen. The UV-Vis-NIR absorption spectra of polymers were recorded on a Thermo Scientific GENESYS™ 10S VIS spectrophotometer. Polymer solutions containing an acid were prepared by adding an intended amount of

acid (TFA, AcOH, or BBr_3) in chlorobenzene under N_2. The molar concentration of the pyrimido[4,5-*g*]quinazoline-4,9-dione (PQ) units of the polymer was kept at $\sim 1 \times 10^{-5}$ M. Cyclic voltammetry (CV) data were obtained on a CHI600E electrochemical analyser using an Ag/AgCl reference electrode and two Pt disk electrodes as the working and counter electrodes in a 0.1 M tetrabutylammonium hexafluorophosphate solution in anhydrous acetonitrile at a scan rate of 50 mV s^{-1}. Ferrocene was used as the reference, which has a HOMO energy level of −4.8 eV.[48] NMR data were recorded on a Bruker DPX 300 MHz spectrometer with chemical shifts relative to the residual $CHCl_3$ in the deuterated solvent (7.26 ppm for $CHCl_3$).[49] Reflection X-ray diffraction (XRD) diagrams of polymer thin films (~40 nm) spin-coated on dodecyltrichlorosilane-modified SiO_2/Si substrates and annealed at 100, 150, 200 °C for 15 min in nitrogen were obtained using a Bruker D8 Advance powder diffractometer with Cu Kα radiation (λ = 0.15406 nm). Transmission XRD measurements were carried out on a Bruker Smart 6000 CCD 3-circle D8 diffractometer with a Cu Kα (Rigaku) X-ray source (λ = 0.15406 nm) using polymer flakes stacked between two Mylar film substrates. Atomic force microscopy (AFM) images were taken on polymer thin films spin-coated on the dodecyltrichlorosilane modified SiO_2/Si substrates with a Dimension 3100 scanning probe microscope. Density functional theory (DFT) through Gaussian 09 Revision D.01[33] using the functional B3LYP and the basis set 6-31G(d) under tight convergence to investigate the geometry, molecular energy levels, and electron distributions for the model compounds.

Synthesis of 3,8-bis(4-octadecyldocosyl)-2,7-di(thiophen-2-yl)-3,8-dihydropyrimido[4,5-*g*]quinazoline-4,9-dione (PQ2T-40)

A 100 mL two-neck round-bottom flask was charged with **PQ2T-H** (0.11 g, 0.29 mmol) and potassium carbonate (0.12 g, 0.88 mmol) and purged with argon. *N*,*N*-Dimethylformamide (DMF) (6 mL) was added and the reaction mixture was heated to 130 °C and stirred for 1 h before 19-(3-iodopropyl)heptatriacontane (0.60 g, 0.88 mmol) was added. The reaction mixture was stirred at the same temperature for an additional 16 h. After cooling, the reaction mixture was extracted with chloroform and the separated organic phase was washed with water. The combined organic phases were dried and the solvent was removed. The residue was purified by column chromatography using 33% chloroform in hexanes to give a yellow liquid, which was treated with isopropanol three times to afford a yellow solid (0.29 g, 66%). ^{1}H-NMR (300 MHz, $CDCl_3$) δ 8.78 (br, 2H), 8.18 (br, 2H), 7.54 (d, J = 5.1 Hz, 2H), 7.20 (t, J = 4.5 Hz, 2H), 4.72 (t, J = 6.7 Hz, 4H), 1.95 (d, J = 7.8 Hz, 4H), 1.59–1.20 (m, 142 H), 0.87 (t, J = 6.5 Hz, 12H). ^{13}C-NMR (75 MHz, $CDCl_3$) δ 167.06, 156.62, 147.43, 144.21, 130.19, 129.54, 128.27, 122.84, 120.08, 68.41, 37.38, 33.78, 32.10, 30.33, 30.07, 29.92, 29.88, 29.53, 26.90, 26.08, 22.86, 14.28. MS (ESI^+) $[M + H]^+$: 1500.7.

Synthesis of 2,7-bis(5-bromothiophen-2-yl)-3,8-bis(4-octadecyldocosyl)-3,8-dihydropyrimido[4,5-*g*]quinazoline-4,9-dione (PQ2T-Br-40)

A 100 mL two-neck round-bottom flask was charged with **PQ2T-40** (0.23 g, 0.16 mmol) and chloroform (14 mL). The reaction mixture was cooled to 0 °C and *N*-bromosuccinimide (NBS) (0.072 g, 0.41 mmol) was added. The reaction mixture was gradually warmed to room temperature and a catalytic amount of bromine was used to accelerate bromination. After stirring overnight in the absence of light, the reaction mixture was washed with a sodium sulfite solution and water, and then dried over sodium sulfate. Purification using column chromatography with a mixture of 25% dichloromethane in hexanes afforded a brown solid (0.21 g, 80%). ^{1}H-NMR (300 MHz, $CDCl_3$) δ 8.72 (s, 2H), 7.92 (br, 2H), 7.14 (d, J = 4.0 Hz, 2H), 4.69 (t, J = 6.7 Hz, 4H), 1.96 (d, J = 8.9 Hz, 4H), 1.70–0.97 (m, 142H), 0.88 (t, J = 6.2 Hz, 12H). ^{13}C-NMR (75 MHz, $CDCl_3$) δ 166.99, 155.56, 147.21, 145.32, 131.36, 129.42, 122.82, 120.03, 117.72, 68.54, 37.33, 33.74, 32.10, 30.33, 29.90, 29.54, 26.89, 25.99, 22.86, 14.29. HRMS (ESI^+) calculated for $C_{98}H_{168}Br_2N_4O_2S_2$ $(M + H)^+$: 1656.1054 found 1656.1036.

Synthesis of PPQ2T-BT-24

To a 25 mL Schlenk flask, **PQ2T-Br-24** (110.0 mg, 0.091 mmol), 5,5′-bis(trimethylstannyl)-2,2′-bithiophene (44.7 mg, 0.091 mmol) and tri(*o*-tolyl)phosphine (P(*o*-tolyl)$_3$) (2.2 mg, 0.007 mmol) were charged. After degassing and refilling argon three times, chlorobenzene (3 mL) and tris(dibenzylideneacetone)-dipalladium ($Pd_2(dba)_3$) (1.7 mg, 0.002 mmol) were added. The reaction mixture was stirred at 130 °C for 72 h. Upon cooling to room temperature, the reaction mixture was poured into methanol (100 mL). The precipitate was collected by filtration and subjected to Soxhlet extraction with acetone, hexanes, and chloroform successively. Further treatment with 1,1,2,2-tetrachloroethane was required to give **PPQ2T-BT-24** upon removal of solvent *in vacuo*. Yield: 105 mg (95%). ^{1}H-NMR spectrum is provided in ESI.†

Synthesis of PPQ2T-BT-40

To a 25 mL Schlenk flask, **PQ2T-Br-40** (100.7 mg, 0.061 mmol), 5,5′-bis(trimethylstannyl)-2,2′-bithiophene (29.9 mg, 0.061 mmol) and P(*o*-tolyl)$_3$ (1.5 mg, 0.005 mmol) were charged. After degassing and refilling argon three times, chlorobenzene (3 mL) and $Pd_2(dba)_3$ (1.1 mg, 0.001 mmol) were added. The reaction mixture was stirred at 130 °C for 72 h. Upon cooling to room temperature, the reaction mixture was poured into methanol (100 mL). The precipitate was collected by filtration and subject to Soxhlet extraction with acetone and hexanes successively. The residual was dissolved in chloroform to give **PPQ2T-BT-40** upon removal of solvent *in vacuo*. Yield: 75 mg (74%). ^{1}H-NMR spectrum is provided in ESI.†

Fabrication and characterization of organic thin film transistors (OTFTs)

A bottom-gate, bottom-contact configuration was used for all OTFT devices. The device fabrication procedure is as follows. A heavily n++-doped SiO_2/Si wafer with ~300 nm-thick SiO_2 was patterned with gold source and drain pairs by conventional photolithography and thermal deposition techniques. Subsequently, the substrate was treated with O_2-plasma, followed by cleaning with acetone and then isopropanol in an ultrasonicating bath. Then the substrate was placed in a solution of dodecyltrichlorosilane in toluene (10 mg mL^{-1}) at room

temperature for 20 min, followed by washing with toluene and drying under a nitrogen flow. A polymer solution in 1,1,2,2-tetrachloroethane (10 mg mL^{-1} for **PPQ2T-BT-24**) or chloroform (5 mg mL^{-1} for **PPQ2T-BT-40**) was spin-coated onto the substrate at 3000 rpm for 60 s to give a polymer film ($\sim$40 nm), which was further subjected to thermal annealing at various temperatures for 30 min in a glove box. All the OTFT devices have a channel length (L) of 30 μm and a channel width (W) of 1000 μm. Devices were characterized in the same glove box using an Agilent B2912A Semiconductor Analyser. The reported mobility (μ) values were calculated using the saturated regime current–voltage characteristics with the drain–source current (I_{DS}) given by:

$$I_{DS} = \left(\frac{WC_i}{2L}\right)\mu(V_G - V_{th})^2$$

where C_i is the capacitance per unit area of the dielectric (11.6 nF cm^{-2}), W (1000 μm) and L (30 μm) are OTFT channel width and length, V_G is the gate voltage, and V_{th} is the threshold voltage.

Conclusions

In summary, two π-conjugated polymers **PPQ2T-BT-24** and **PPQ2T-BT-40** based on a new building block, pyrimido[4,5-*g*]-quinazoline-4,9-dione (PQ), were synthesized. These polymers showed significant bathochromic shifts in their absorption profiles in the presence of protonic (acetic acid and trifluoroacetic acid) and Lewis (BBr_3) acids, resulting from the strong interaction of the basic 1,6-nitrogen atoms in the PQ unit with the acid. As an active channel layer in OTFTs, these polymers exhibited characteristic p-type semiconductor performance with hole mobility as high as 6.4×10^{-3} cm^2 V^{-1} s^{-1}. Our preliminary results demonstrate that PQ is a promising new building block for polymer semiconductors. The chemo- and bio-sensing capabilities of these polymers will be studied and reported in due course.

Acknowledgements

The financial support of this work from the Natural Sciences and Engineering Research Council (NSERC) of Canada (Discovery Grants #402566-2011) is greatly acknowledged.

Notes and references

1 G. Horowitz, *Adv. Mater.*, 1998, **10**, 365–377.
2 C. D. Dimitrakopoulos and P. R. L. Malenfant, *Adv. Mater.*, 2002, **14**, 99–117.
3 H. Klauk, *Chem. Soc. Rev.*, 2010, **39**, 2643–2666.
4 P. Lin and F. Yan, *Adv. Mater.*, 2012, **24**, 34–51.
5 L. Torsi, M. Magliulo, K. Manoli and G. Palazzo, *Chem. Soc. Rev.*, 2013, **42**, 8612–8628.
6 B. Kumar, B. K. Kaushik and Y. S. Negi, *Polym. Rev.*, 2014, **54**, 33–111.
7 C. Zhang, P. Chen and W. Hu, *Chem. Soc. Rev.*, 2015, **44**, 2087–2107.
8 X. Guo, A. Facchetti and T. J. Marks, *Chem. Rev.*, 2014, **114**, 8943–9021.
9 A. Pron and M. Leclerc, *Prog. Polym. Sci.*, 2013, **38**, 1815–1831.
10 Y. Li, P. Sonar, L. Murphy and W. Hong, *Energy Environ. Sci.*, 2013, **6**, 1684–1710.
11 Y. He, W. Hong and Y. Li, *J. Mater. Chem. C*, 2014, **2**, 8651–8661.
12 H. Yan, Z. Chen, Y. Zheng, C. Newman, J. R. Quinn, F. Dötz, M. Kastler and A. Facchetti, *Nature*, 2009, **457**, 679–686.
13 Y. Li, S. P. Singh and P. Sonar, *Adv. Mater.*, 2010, **22**, 4862–4866.
14 T. Lei, Y. Cao, Y. Fan, C. J. Liu, S. C. Yuan and J. Pei, *J. Am. Chem. Soc.*, 2011, **133**, 6099–6101.
15 Z. Yan, B. Sun and Y. Li, *Chem. Commun.*, 2013, **49**, 3790–3792.
16 T. Lei, X. Xia, J. Y. Wang, C. J. Liu and J. Pei, *J. Am. Chem. Soc.*, 2014, **136**, 2135–2141.
17 H. S. a. Al-Salem, G. H. Hegazy, K. E. H. El-Taher, S. M. El-Messery, A. M. Al-Obaid and H. I. El-Subbagh, *Bioorg. Med. Chem. Lett.*, 2015, **25**, 1490–1499.
18 R. Bouley, M. Kumarasiri, Z. Peng, L. H. Otero, W. Song, M. A. Suckow, V. A. Schroeder, W. R. Wolter, E. Lastochkin, N. T. Antunes, H. Pi, S. Vakulenko, J. A. Hermoso, M. Chang and S. Mobashery, *J. Am. Chem. Soc.*, 2015, **4**, 3–6.
19 W. Lu, I. A. Baig, H.-J. Sun, C.-J. Cui, R. Guo, I.-P. Jung, D. Wang, M. Dong, M.-Y. Yoon and J.-G. Wang, *Eur. J. Med. Chem.*, 2015, **94**, 298–305.
20 S. Oschatz, T. Brunzel, X. Wu and P. Langer, *Org. Biomol. Chem.*, 2015, **13**, 1150–1158.
21 K. Zhu, J. Hao, C. Zhang, J. Zhang, Y. Feng and H. Qin, *RSC Adv.*, 2015, **5**, 11132–11135.
22 L.-P. Peng, S. Nagarajan, S. Rasheed and C.-H. Zhou, *Med. Chem. Commun.*, 2015, **6**, 222–229.
23 J. T. Mabeck and G. G. Malliaras, *Anal. Bioanal. Chem.*, 2005, **384**, 343–353.
24 C. Liao and F. Yan, *Polym. Rev.*, 2013, **53**, 352–406.
25 C. Liao, M. Zhang, M. Y. Yao, T. Hua, L. Li and F. Yan, *Adv. Mater.*, 2014, 1–35.
26 M. T. Bogert and A. W. Dox, *J. Am. Chem. Soc.*, 1905, **27**, 1127–1140.
27 M. T. Bogert and J. M. Nelson, *J. Am. Chem. Soc.*, 1907, **29**, 729–739.
28 W. Med and K. Johne, *Z. Chem.*, 1970, **10**, 397–398.
29 E. B. Skibo and J. H. Gilchrist, *J. Org. Chem.*, 1988, **53**, 4209–4218.
30 R. H. Lemus and E. B. Skibo, *J. Org. Chem.*, 1992, **57**, 5649–5660.
31 E. B. Skibo, X. Huang, R. Martinez, R. H. Lemus, W. a. Craigo and R. T. Dorr, *J. Med. Chem.*, 2002, **45**, 5543–5555.
32 J. Quinn, E. Jin and Y. Li, *Tetrahedron Lett.*, 2015, **56**, 2280–2282.
33 M. J. Frisch, *et al.*, *Gaussian 09 Revision D.01*, Gaussian, Inc., Wallingford, CT, USA, 2009, see full citation in ESI†.
34 S. Chen, B. Sun, W. Hong, H. Aziz, Y. Meng and Y. Li, *J. Mater. Chem. C*, 2014, **2**, 2183.
35 F. C. Spano and C. Silva, *Annu. Rev. Phys. Chem.*, 2014, **65**, 477–500.

36 H. Yamagata and F. C. Spano, *J. Chem. Phys.*, 2012, **136**, 184901–184914.
37 T. Yasuda and T. Yamamoto, *Macromolecules*, 2003, **36**, 7513–7519.
38 T. Yamamoto, T. Uemura, A. Tanimoto and S. Sasaki, *Macromolecules*, 2003, **36**, 1047–1053.
39 T. Yamamoto, K. Sugiyama, T. Kanbara, H. Hayashi and H. Etori, *Macromol. Chem. Phys.*, 1998, **199**, 1807–1813.
40 I. Nurulla, A. Tanimoto, K. Shiraishi, S. Sasaki and T. Yamamoto, *Polymer*, 2002, **43**, 1287–1293.
41 I. Nurulla, K. Sugiyama, B.-L. Lee and T. Yamamoto, *React. Funct. Polym.*, 2000, **46**, 49–53.
42 G. C. Welch and G. C. Bazan, *J. Am. Chem. Soc.*, 2011, **133**, 4632–4644.
43 T. Tang, T. Lin, F. Wang and C. He, *Polym. Chem.*, 2014, **5**, 2980.
44 C. A. Matuszak and A. J. Matuszak, *J. Chem. Educ.*, 1976, **53**, 280.
45 J.-S. Yang and T. M. Swager, *J. Am. Chem. Soc.*, 1998, **120**, 11864–11873.
46 M. J. Winokur, D. Spiegel, Y. Kim, S. Hotta and A. J. Heeger, *Synth. Met.*, 1989, **28**, 419–426.
47 *WO. Pat.*, 2014071524 A1, 2014.
48 J. Pommerehne, H. Vestweber, W. Guss, R. F. Mahrt, H. Bassler, M. Porsch and J. Daub, *Adv. Mater.*, 1995, **7**, 551–554.
49 H. E. Gottlieb, V. Kotlyar and A. Nudelman, *J. Org. Chem.*, 1997, **62**, 7512–7515.

